# Mechanism Analysis on Radio Frequency Radiation in IC/Package with Bonding Wires

Muqi Ouyang<sup>1</sup>, Yin Sun<sup>1</sup>, Jongjoo Lee<sup>1</sup>, Jingook Kim<sup>2</sup> and Chulsoon Hwang<sup>1</sup>

<sup>1</sup>Missouri S&T EMC Laboratory Missouri University of Science and Technology Rolla, MO, USA hwange@mst.edu <sup>2</sup>Ulsan National Institute of Science and Technology Ulsan, Korea

Abstract—IC/package radiation from a self-designed inverter chip bonded to a PCB was measured, and the radiation mechanism was investigated. Digital signals from ICs can have wide-spread frequency spectrums, and radiated signals in the radio frequency range can be picked up by other radio receivers, which causes radio-frequency interference problems. First, an equivalent radiation source for an inverter chip bonded to a PCB is reconstructed based on near-field patterns measured above the chip. The validity of the reconstructed source is proved by comparing the coupled voltage measured on a victim antenna and the voltage calculated based on the reconstructed radiation source. Then, the radiation mechanism is investigated by analyzing the equivalent radiation source as well as the signal and return current paths in full-wave simulations. Then, the critical current paths responsible for the radiation are identified. Finally, a simplified model is proposed to calculate the equivalent radiation source, with which the errors between the simplified model and full-wave simulation results were found to be within 5%.

Keywords—bonding wire, radio-frequency interference, radiation mechanism

### I. INTRODUCTION

Digital signals input to or output from digital ICs contain wide-spread frequency spectrums. The radiated signals in the radio frequency (RF) range can be picked up by radio receivers nearby, which results in RF desensitization on the receivers [1]. Therefore, digital ICs are usually a primary source for many RF interference problems in modern electronic devices. Understanding the radiation mechanism is important in terms of analyzing IC/package level radiation problems and optimizing designs for lower radiation levels.

Wire bonds are commonly used as 1<sup>st</sup>-level interconnections between ICs. Generally, as the return current paths are not well-guided in the bonding wire area, the bonding wire structures are the most representative radiation structures at the chip/package level. However, in practical cases, analyzing the radiation mechanism for bonding wires can be difficult because the number of bonding wires can be large and bonding wires for signal and power/GND may be alternating.

In [2], a closed-form solution for bonding wire radiation pattern is proposed. However, the mathematical derivations only include the current on one bonding wire, and the return path is not considered. There has been much research and applications for using bonding wires as chip level antennas, where the bonding wires are designed to be good radiators [3, 4]. Generally, in these applications, the radiating structures are designed intentionally and are easier to analyze compared to the unintentional radiation from digital ICs, where the current paths are difficult to identify. In [5, 6], the radiation pattern from an IC/package with bonding wires or a flip-chip interconnect was investigated, but the investigations were focused on much higher frequency ranges compared to the RF range. Also, methods to estimate interference in the RF or other frequency ranges from the IC/package are not discussed in these studies.

In this paper, the radiation from a self-designed IC bonded directly to a PCB was measured, and an equivalent radiation source was reconstructed based on the near-field patterns above the IC. The coupled voltages at the victim antenna port can be calculated using the reconstructed radiation source and the results have a good correlation to the measurement results. Then, the radiation mechanism of the IC with bonding wires was investigated by analyzing the signal and the return current paths in full-wave simulations. Based on the understanding of the radiation mechanism, a simplified radiation model is proposed, and methods to lower the radiation from the IC/package by modifying the bonding wire designs are introduced.

## II. EQUIVALENT SOURCE FOR RF INTERFERENCE

When ICs are populated on the PCB, which is usually a part of the embedded RF antenna, the coupling between the antenna and ICs occurs in the near-field region. To analyze the radiation mechanism and RF interference resulting from an IC with bonding wires, the radiating IC structure and the victim antenna need to be investigated together in either measurements or full-wave simulations. However, based on the reciprocity theorem, the RF interference can be decomposed into two independent parts: the equivalent radiation source from the radiator and the radiated field from the victim antenna in the reverse problem using (1) [7, 8, 9].

$$V_{coupled} = \frac{Z_L}{2} \cdot \frac{H_{i,rev}}{V_{rev}^+} \cdot M_i \tag{1}$$

Where  $Z_L$  is the load impedance of the RF receiver (usually 50 Ohms);  $V_{rev}^+$  and  $H_{i,rev}$  are the incident voltage at the antenna port and the magnetic field at the noise source location

This paper is based upon work supported partially by the National Science Foundation under Grant No. IIP-1916535.

in the reverse problem; and  $M_i$  is the equivalent dipole representing the IC radiation.  $H_{i,rev}$  /  $V_{rev}^+$  and  $M_i$  represents characteristics of the antenna and IC radiation, respectively. For the self-designed inverter chip bonded to the PCB, the equivalent radiation source reconstructed based on the near-field patterns is a single magnetic dipole, which is shown later in this paper. Therefore, in (1), only a single magnetic dipole needs to be included in the calculation.

Based on (1), IC radiation mechanism analysis and modeling can be carried out independently, and then combined with the antenna fields later, which greatly simplifies the problem. The validity of (1) is demonstrated in this section using a real IC with an embedded antenna integrated on the same board.

#### A. DUT and Measurement Descriptions

To investigate the radiation resulting from a chip/package design, a chip with an inverter chain was designed and connections between on-die pins and PCB pads were made directly through bonding wires, as shown in Fig. 1. If the on-die pads and bonding wires for the input and output signals are near one another on the same edge, it is difficult to distinguish

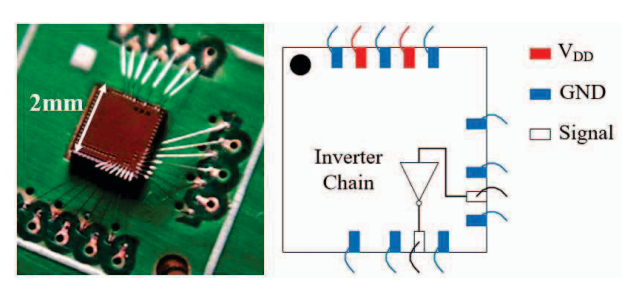
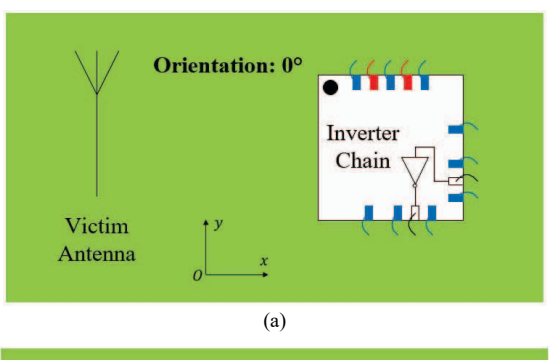


Fig. 1. A photo of the fabricated IC and the bonding configuration.



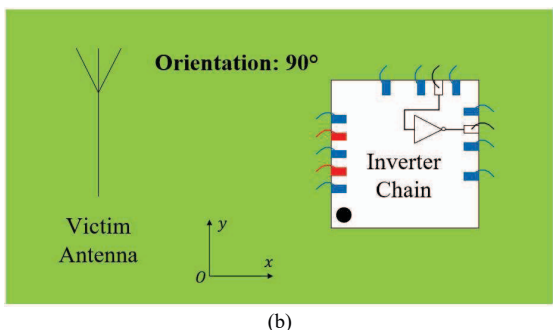


Fig. 2. Designed PCBs with different IC orientation; (a) 0° rotation (b) 90° rotation.

the input and output signals and their return paths from radiation measurements. To avoid this issue, the input and output wire bonds are placed orthogonally. There are GND pins on both sides of all the input and output signal pins of the inverter chain to ensure good current return paths for high-speed signals.

To avoid radiations caused by PCB trace routings and other PCB components, all signal traces on the PCB are routed as striplines and connected to the bonding wire pads through vias locating next to those pads. In addition, all SMA connectors, bulk capacitors, and power input pins on the PCB are shielded. Therefore, only the chip and its bonding wires can radiate effectively. A PIFA (Planar Inverted-F Antenna) with an SMA port was also designed on the PCB and the antenna can receive signals effectively from 700 MHz to 900 MHz. The antenna has a common ground with the IC on the PCB to mimic realistic products. A simplified figure demonstrating the PCB structure is shown in Fig. 2. There are two chip orientations, 0° and 90°.

In the measurements, the output of the inverter chain is terminated with 50 Ohms. To measure the radiation behavior at frequency  $f_0$ , a sinusoidal signal at  $0.5f_0$  with  $0.5V_{\rm DD}$  DC bias is used as the input of the inverter, instead of a square wave.  $V_{\rm DD}$  is the DC power level for the chip. Therefore, when measuring at frequency  $f_0$ , only the driver's output current (and return current) will contribute to radiation.

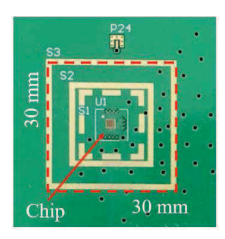


Fig. 3 Scanning area above the chip (30 mm by 30 mm)

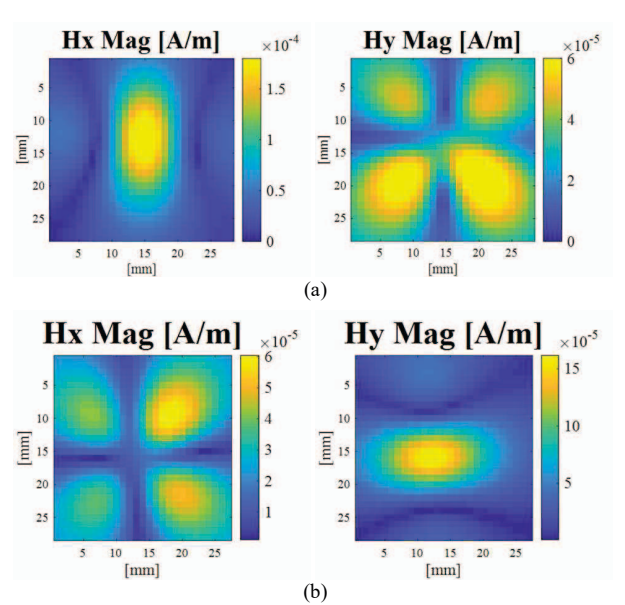


Fig. 4. Measured H-field patterns at 800 MHz (a)  $0^{\circ}$  rotation (b)  $90^{\circ}$  rotation.

## B. Equivalent Radiation Source Reconstruction

Near-field scanning was carried out to reconstruct the dipole moment. The scanning area of the near-field pattern is 30 mm by 30 mm and the scanning height is 9 mm above the PCB. A spectrum analyzer with an H-field probe was used to measure the magnitudes of the near-fields, and the measured values are converted to magnetic field values through probe calibration [10]. The scanning area is shown in Fig. 3, and the scanned results are shown in Fig. 4.

The measured near-field patterns above the IC for  $0^{\circ}$  rotation are close to the patterns generated by a magnetic dipole in the x direction, while the patterns above the IC for  $90^{\circ}$  rotation are close to the patterns generated by a magnetic dipole in the y direction. Therefore, based on these near-field patterns, the radiation source of the inverter chip with bonding wires can be reasonably modeled as an equivalent magnetic dipole. Then, an equivalent dipole can be reconstructed by using a least square method with magnitude-only data [11].

# C. Coupled Voltage at the Antenna Port

The radio  $H_{i,rev}$  /  $V_{rev}^*$  was measured using a vector network analyzer with an H-field probe. One port was connected to the antenna port and the other was connected to the H-field probe. As the dipole moment  $M_i$  was already reconstructed in the previous section, all the necessary information to calculate the coupled voltage at the antenna port is obtained, and the coupled voltage at the antenna port can be calculated using (1). The comparisons between the coupled voltages from measurements and the reconstructed source calculations at the victim antenna port from 700 MHz to 900 MHz are shown in Fig. 5.

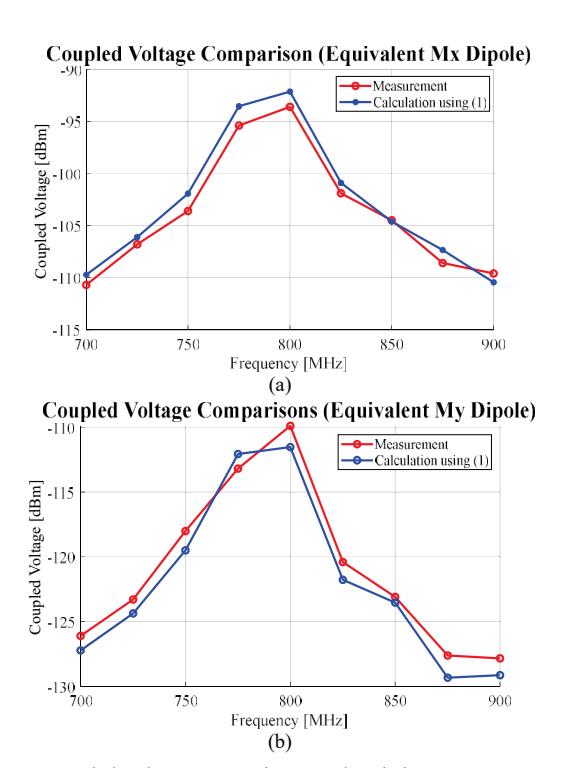


Fig. 5. Coupled voltages comparisons at the victim antenna port with equivalent magnetic dipole (a) 0° rotation (b) 90° rotation.

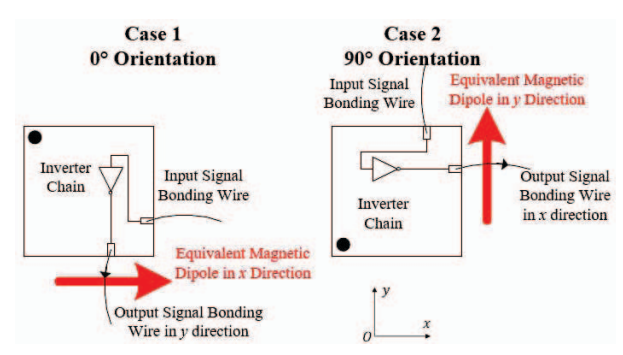


Fig. 6. Directions of the signal bonding wires and equivalent magnetic dipole sources.

With the equivalent magnetic dipole source in either the x or y direction, the differences between the measured voltages at the antenna port and the calculated voltages from the reconstructed equivalent source are less than 2 dB. Therefore, using an equivalent magnetic dipole to model the radiation from the bonding wire of the output signal on this inverter chip is validated.

#### III. ANALYSIS ON RADIATION MECHANISM

Notice that the direction of the equivalent magnetic dipole is perpendicular to the direction of the output signal bonding wire (as shown in Fig. 6), which indicates that the radiations are able to be related to a current loop including the output signal bonding wire and the PCB ground plane beneath the bonding wires. However, as shown in Fig. 1, on both sides of the input and output signal bonding wires, there are GND bonding wires, which should be the current path with the least impedance. On the other side, due to the silicon substrate between the on-die circuits and the PCB, there is no good direct path for conductive currents between the on-die ground and the PCB ground through the silicon substrate.

The signal current and the return currents on the adjacent GND bonding wires make 2 current loops, which result in a magnetic dipole in the +z direction and another magnetic dipole in the -z direction. Due to the image effect from the PCB ground and the cancelation between these 2 magnetic dipoles in opposite directions, these 2 current loops will not generate large radiations. If all the signal current returns from these adjacent GND bonding wires, the radiation from the signal current should be mostly cancelled, and the magnetic dipole perpendicular to the signal bonding wire should not be observed. Thus, careful investigations on the current paths are needed in full-wave simulations to understand the radiation mechanism.

#### A. Near-field Patterns from Full-Wave Simulations

To investigate the radiation from these bonding wire structures, a full-wave model with similar geometry to the self-designed chip and its bonding wire structures were simulated. For simplicity in simulations, a large ground plane is used to connect all the on-die ground bonding wires, and there is a layer of silicon dioxide with 0.01 mm thickness and a layer of silicon with 0.3 mm thickness beneath the on-die ground plane. Because of the sinusoidal input signal to the inverter, the radiation at the harmonic frequency concentrates on the output signal bonding wire. Thus, only one output signal bonding wire and the other

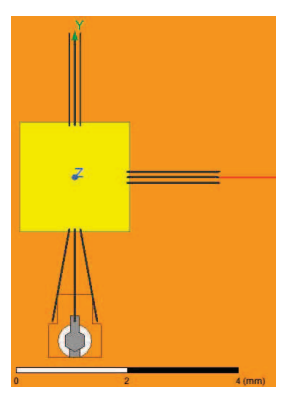


Fig. 7. Top view of the full-wave simulation model for radiation mechanism analysis.

ground bonding wires are included in the model. For the output bonding wire, there is a 1-A current source on the on-die side and a via transition to a 50-Ohm stripline on the PCB side, as shown in Fig. 7. Apart from the ground bonding wires next to the signal bonding wire on the bottom edge of the chip, 3 more ground bonding wires are added on both the right edge and the top edge of the chip, which are based on the actual bonding wire structure of the self-designed chip.

The near-field patterns from the full-wave simulation are shown in Fig. 8. In the simulation model, the direction of the output signal bonding wire is the same as the measurement case shown in Fig. 2(a). The obtained near-field patterns are shown in Fig. 8, which are also similar to the patterns generated by a magnetic dipole in the *x* direction. Because the output current source in the simulation is different as compared to the output from an actual on-die inverter, there are differences in magnitudes, which is not of interest here. Similar near-field patterns between the simulation and measurement results indicate that the simulation model is representative of the actual chip, and analyzing the simulation model can help understand the radiation mechanism.

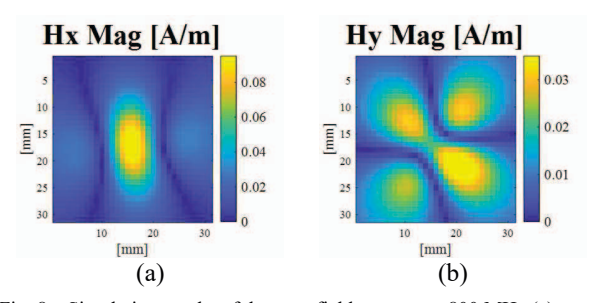


Fig. 8. Simulation results of the near-field patterns at 800 MHz (a) magnitude of  $H_x$  field; (b) magnitude of  $H_y$  field.

# B. Understanding of Current Path and Simplified Model

The surface current distribution on the PCB ground plane from simulation is shown in Fig. 9. Notice that apart from the area beneath the signal bonding wire and the GND bonding wires on the same side of the chip, the surface currents are also concentrated beneath the GND bonding wires on other edges, which are much further away compared to the GND bonding wires next to the signal bonding wire. The current distribution on the PCB ground plane indicates that the signal current returns

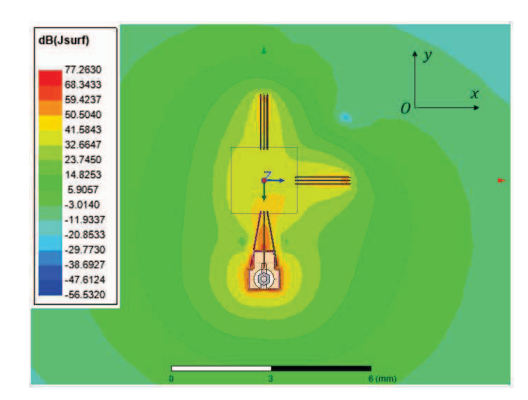


Fig. 9. Top view of surface current distributions on the top layer of the PCB ground in log scale.

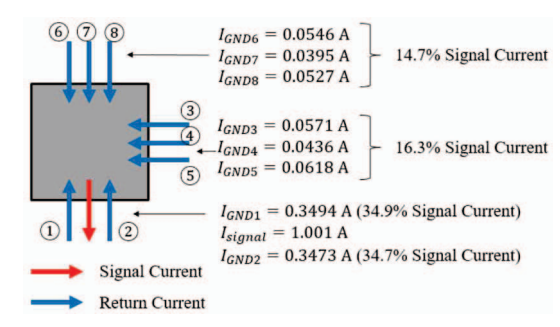


Fig. 10. Currents on each bonding wire at 800 MHz

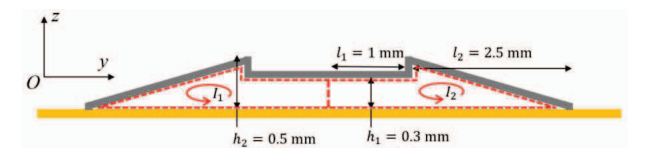


Fig. 11. Side view of the simplified bonding wires model and current loops.

not only from the neighboring GND bonding wires, but also from other GND bonding wires. This is the key to explaining the direction of the magnetic dipole. To quantitatively show that there are currents returning from other GND bonding wires, the current on each bonding wire is calculated by Ampere's law using the magnetic fields around these bonding wires, and the calculation results are shown in Fig. 10.

Although most of the output signal currents return from the GND signal bonding wires next to the signal bonding wire (which does not contribute to radiation!), currents returning from other GND bonding wires are not negligible. These currents returning from other GND bonding wires are the main contributors to the measured magnetic dipole, the near-field patterns measured above the IC, and the coupled voltage measured at the victim antenna port.

Based on the near-field patterns above the IC (Fig. 8), the equivalent magnetic dipole can be reconstructed using the least square method and the magnitude of the equivalent magnetic dipole in the *x* direction is:

$$|M_x| = 0.4369 \ \mu \text{A} \cdot \text{m}^2$$

Also, the magnitude of a magnetic dipole is equal to the current magnitude times the area of the current loop. So, an equivalent magnitude dipole can be calculated based on the currents on the bonding wires (Fig. 10) and the areas of these current loops. Since the equivalent source is a magnetic dipole in the *x* direction, only the current loops in the *x* direction are considered, and the simplified side view is shown in Fig. 11. The area of each current loop is:

$$S = l_1 h_1 + \frac{1}{2} l_2 h_2 = 0.925 \text{ mm}^2$$
 (2)

The current magnitude in each loop is:

$$I_1 = I_{\text{signal}} - I_{\text{GND1}} - I_{\text{GND2}} = 0.3043 \text{ A}$$
 (3)

$$I_2 = I_{\text{GND6}} + I_{\text{GND7}} + I_{\text{GND8}} = 0.1468 \text{ A}$$
 (4)

So, the magnitude of the equivalent magnetic dipole in the *x* direction is:

$$|M_x| = (I_1 + I_2) \cdot S = 0.4173 \ \mu \text{A} \cdot \text{m}^2$$
 (5)

The equivalent magnetic dipole calculated from (5), based on the simplified current loop model, is close to the equivalent source reconstructed from the simulated near-field patterns, which indicates that the radiation from the chip is related to bonding wire loops and current returns from other edges of the chip.

Therefore, the current returning from the GND bonding wires on the other edges of the chip is the dominant contributor to the radiation because: 1) the current returning from other edges of the chip makes the current on the neighboring GND bonding wires smaller, resulting in a weaker cancellation to the radiation from the output signal current; 2) the current return path including the GND bonding wires on the other edges is a large loop, and this loop current can radiate effectively.

Although the current returning from the GND bonding wires on other edges of the chip is only about half of the GND currents on the bonding wires next to the signal output, effective radiation behaviors from the IC/package and bonding wire structures can be observed.

#### C. Bonding Wire Designs with Lower Radiation

Based on the understanding of the radiation mechanism, design implications can be developed for low radiation and to alleviate RF interference issues. Two bonding wire design examples are shown in Fig. 12. For clarity purposes, let the original bonding wire design (shown in Fig. 10) be Case 1, the design without bonding wires on the right edge of the chip (Fig. 12(a)) be Case 2, and the design without bonding wires on the right and the top edges (Fig. 12(b)) be Case 3. The current magnitudes on all bonding wires at 800 MHz are extracted from full-wave simulation results.

The reconstructed magnetic dipole sources based on the simulated near-field patterns can be found in TABLE I. For Case 1 and Case 2, the calculations are based on the simplified model (Fig.11) and (2)-(5). For Case 3, the current loop is assumed to be the loop for  $I_1$  in Fig. 11, and the loop for  $I_2$  does not exist. The magnitudes of the reconstructed sources in Case 1 and Case 2 are similar, but the reconstructed source in Case 3 greatly

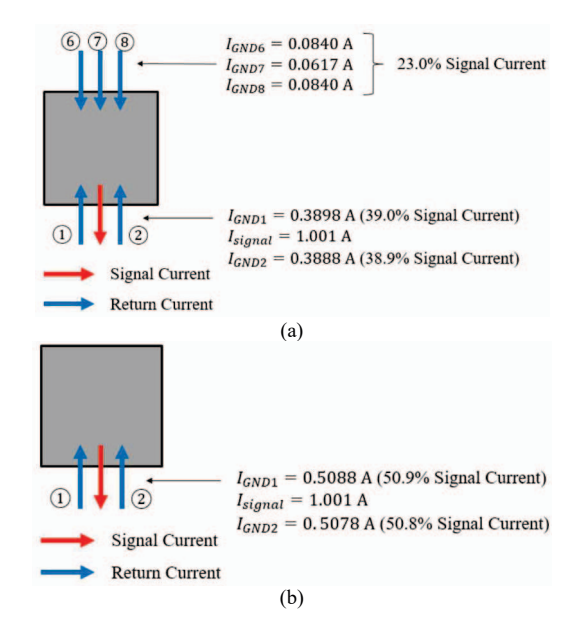


Fig. 12. Examples on altering bonding wire design to achieve lower radiation (a) Case 2: GND bonding wires on the right edge are removed; (b) Case 3: GND bonding wires on the right and the top edges are removed.

TABLE I. MAGNITUDES OF RECONSTRUCTED MAGNETIC DIPOLE SOURCES IN DIFFERENT BONDING WIRE DESIGNS AT 800 MHz

	Case 1	Case 2	Case 3
Equivalent Magnetic Dipole Source from Near-Field Patterns $\left[ \ \mu A \cdot m^2 \ \right]$	0.4369	0.4193	0.0943
Equivalent Magnetic Dipole Source from Analytical Calculation using the Simplified Model $\left[\begin{array}{c}\mu A\cdot m^2\end{array}\right]$	0.4173	0.4182	0.0144

decreases compared to the other 2 cases. Therefore, the bonding wire design in Case 3 has a lower radiation level compared to the other 2 cases, and the RF interference at the victim antenna port will also be lower because of the lower equivalent source. It is worth noting that all bonding wires on the same edge have less radiation than the bonding wires distributed on different edges, especially those on the opposite-side edge.

For both Case 1 and Case 2, the differences between the magnetic dipole reconstructed based on simulated near-field patterns and the magnetic dipole from analytical calculation are within 5%. However, the difference is much larger for Case 3.

In Case 3, most of the current returns from the adjacent GND bonding wires, so the equivalent magnetic dipole calculated analytically from the simplified model is much weaker. However, in the full-wave model, there are some top-layer transition structures between the signal bonding wire and the 2<sup>nd</sup>-layer stripline. As shown in Fig. 13, the center of the near-field patterns in full-wave simulation for Case 3 moves to the top of these transition structures, which indicates that these PCB transition structures become the dominant contributors to the radiation shown in the near-field patterns. This part of the radiation is not included in the simplified radiation model, and

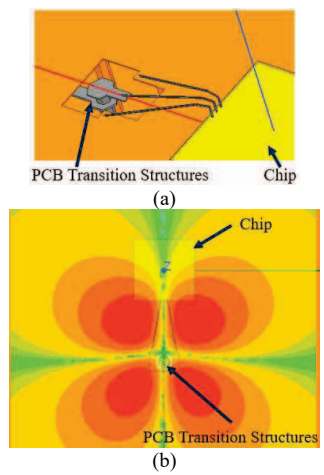


Fig. 13 (a) PCB transition structures; (b) Center of the near-field  $|H_y|$  pattern moves to the top of PCB transition structures in Case 3.

this is the reason why the equivalent magnetic dipole reconstructed based on the near-field patterns in Case 3 is significantly larger comparing to the result from the simplified model. In Case 1 and Case 2, the radiation is dominated by the bonding wire structures, rather than by the PCB transition structures, so the simplified radiation model can accurately predict the radiation source.

The radiation behaviors under different configurations of the GND bonding wires are within expectations, and the equivalent radiation sources obtained from near-field pattern fitting and analytical calculation have good agreement. Therefore, the validity of the simplified current loop model for predicting radiation from bonding wire structures is proved. Also, these observations indicate that the analysis and understanding of the radiation mechanism are correct.

Based on the understanding of the radiation mechanism, it can be concluded that controlling the possible return current paths on the bonding wires is important for low-radiation designs. Case 3 has a much lower radiation level comparing to Case 1 and Case 2, because there is no current path for return currents on different edges of the chip, and good radiation cancellation can be achieved on the GSG bonding wire structures. Similarly, if there are multiple signal and GND bonding wires that need to be assigned, a design with all of these bonding wires on the same side of the chip, if it is possible, should have a lower radiation level compared to a design with bonding wires on all different edges of the chip.

#### IV. CONCLUSION

In this paper, the radiations from IC/bonding wire structures are measured, and the radiation mechanism is analyzed through measurement results and full-wave simulations. A simple current path model is proposed and validated to understand the radiation mechanism. It is found that the radiation is dictated by a small return current through all the GND bonding wires. The

large current loops including the GND bonding wires on other edges of the chip contribute to the radiation. Also, because of these additional return current paths, the return current on the neighboring GND bonding wires is less, and the radiation cancellation in the GSG bonding wire structure is weaker. Based on the understanding of the radiation mechanism, design implications for low radiation are discussed. All GND bonding wires can be possible paths for return currents. Keeping all these bonding wires on the same side with the output signal bonding wire is an effective method to mitigate radiation from IC/bonding wire structures.

#### REFERENCES

- Q. Huang et al., "Desense prediction and mitigation from DDR noise source," in 2018 IEEE Symposium on Electromagnetic Compatibility, Signal Integrity and Power Integrity (EMC, SI & PI), 2018, pp. 139-144: IEEE.
- [2] L.-C. Lin, C.-H. Tu, D.-C. Chang, and Y.-Z. Juang, "Radiation pattern estimation of bond wire antennas," in *Proceedings of the 2012 IEEE International Symposium on Antennas and Propagation*, 2012, pp. 1-2: IEEE.
- [3] Q. Liu, U. Johannsen, M. C. van Beurden, and A. Smolders, "Antennaon-Chip Radiation Pattern Characterization—Analysis of Different Approaches," in 2019 13th European Conference on Antennas and Propagation (EuCAP), 2019, pp. 1-5: IEEE.
- [4] I. Ndip, M. Huhn, T. H. Le, and K.-D. Lang, "Double-wired bond wire antennas," in 2018 22nd International Microwave and Radar Conference (MIKON), 2018, pp. 216-217: IEEE.
- [5] M. Hitzler, L. Boehm, W. Mayer, and C. Waldschmidt, "Radiation pattern optimization for QFN packages with on-chip antennas at 160 GHz," *IEEE Transactions on Antennas and Propagation*, vol. 66, no. 9, pp. 4552-4562, 2018.
- [6] H.-C. Lu and Y.-L. Chang, "Radiation pattern measurement assembly for millimeter-wave antenna by flip-chip interconnect and end launch connector," in 2014 Asia-Pacific Microwave Conference, 2014, pp. 131-133: IEEE.
- [7] Y. Sun, B.-C. Tseng, H. Lin, and C. Hwang, "RFI Noise Source Quantification Based on Reciprocity," in 2018 IEEE Symposium on Electromagnetic Compatibility, Signal Integrity and Power Integrity (EMC, SI & PI), 2018, pp. 548-553: IEEE.
- [8] Q. Huang, F. Zhang, T. Enomoto, J. Maeshima, K. Araki, and C. Hwang, "Physics-based dipole moment source reconstruction for RFI on a practical cellphone," *IEEE Transactions on Electromagnetic Compatibility*, vol. 59, no. 6, pp. 1693-1700, 2017.
- [9] Y. Sun, H. Lin, B.-C. Tseng, D. Pommerenke, and C. Hwang, "Mechanism and Validation of USB 3.0 Connector Caused Radio Frequency Interference," *IEEE Transactions on Electromagnetic Compatibility*, 2019.
- [10] Q. Huang, Y. Liu, L. Li, Y. Wang, C. Wu, and J. Fan, "Radio frequency interference estimation using transfer function based dipole moment model," in 2018 IEEE International Symposium on Electromagnetic Compatibility and 2018 IEEE Asia-Pacific Symposium on Electromagnetic Compatibility (EMC/APEMC), 2018, pp. 115-120: IEEE
- [11] Q. Huang et al., "Reciprocity Theorem Based RFI Estimation for Heatsink Emission," in 2019 IEEE International Symposium on Electromagnetic Compatibility, Signal & Power Integrity (EMC+ SIPI), 2019, pp. 590-594: IEEE.
- [12] HyperWorks FEKO, Altair Engineering Inc., http://www.altairhyperworks.com/product/FEKO